


Thermodynamic limit of spin systems on random graphs

Amy Searle¹ and Joseph Tindall^{2,*}

¹*Department of Physics, University of Oxford, Oxford OX1 3PU, United Kingdom*

²*Center for Computational Quantum Physics, Flatiron Institute, 162 5th Avenue, New York, New York 10010, USA*

 (Received 3 March 2023; revised 10 October 2023; accepted 1 December 2023; published 3 January 2024)

We utilize the graphon—a continuous mathematical object which represents the limit of convergent sequences of dense graphs—to formulate a general, continuous description of quantum spin systems in thermal equilibrium when the average coordination number grows extensively in the system size. Specifically, we derive a closed set of coupled nonlinear Fredholm integral equations which governs the properties of the system. The graphon forms the kernel of these equations, and their solution yields exact expressions for the macroscopic observables in the system in the thermodynamic limit. We analyze these equations for both quantum and classical spin systems, recovering known results and providing analytical solutions for a range of more complex cases. We supplement this with controlled, finite-size numerical calculations using Monte Carlo and tensor network methods, showing their convergence towards our analytical results with increasing system size.

DOI: [10.1103/PhysRevResearch.6.013011](https://doi.org/10.1103/PhysRevResearch.6.013011)

I. INTRODUCTION

The physical properties of interacting systems are strongly affected by the connectivity of their components. For instance, network topology plays a decisive role in the rate of disease spreading in infectious disease models [1], while systematic studies have been undertaken on the effect of connectivity on the synchronization of oscillators [2–5].

In interacting spin systems, the same ideas hold true: frustration causes the manifestation of exotic phases of matter such as a spin liquids [6], and small-world effects alter the underlying universality class of ordered-disordered phase transitions [7]. The difficulty of solving the many-body problem (especially in the quantum regime), however, means a more general characterization of how network topology influences strongly correlated systems is unknown.

When disorder is absent and the average coordination number becomes large, interacting many-body systems fall into the mean-field universality class and become amenable to simpler mathematical and computational approaches [8–12]. Despite mostly being applied to translationally invariant systems, the mean-field approach is known to be valid for an infinite multitude of networks, whether homogeneous or heterogeneous [13]. Although it is only exact in the thermodynamic limit and when the average coordination number grows proportionally with the system size [14], mean-field theory can provide meaningful physical predictions for low-dimensional systems [15,16]. Within the field of graph theory, network structures—whether heterogeneous

or homogeneous—with an extensive coordination number are well characterized. Their thermodynamic limit is succinctly described by the graphon [17,18], a continuous mathematical object which represents the limit of a sequence of adjacency matrices as the number of vertices tends to infinity and the average coordination number grows extensively.

Here we utilize the graphon in the study of interacting spin systems. This allows us to formally take the thermodynamic limit and derive an exact, continuous theory for the limit of sequences of discrete Hamiltonian on graphs of increasing size and average coordination number. Specifically, we take a very general spin Hamiltonian defined over an arbitrary graph and, for sequences of dense graphs whose limit is known to converge to a given graphon, derive a coupled set of integral equations which exactly describes the equilibrium physics of the limit of the corresponding sequence of Hamiltonians. The graphon forms the kernel in these integral equations, and the physics of the system can be directly studied as a function of this object.

Taking several classical and quantum example models, we demonstrate the utility of these integral equations, (i) verifying previous results on all-to-all spin systems, (ii) proving the existence of a finite-temperature phase transition in the classical Ising model for any graphon, and (iii) deriving analytical solutions for the equilibrium observables of spin models on nontrivial, heterogeneous networks. We reinforce our analytical solutions with large-scale, finite-size Monte Carlo and tensor network simulations. Although the spin systems we treat in this work are commonly studied due to their relevance as models of real-world magnetism, they also find application in many other branches of science, including the political, social, and biological sciences [19–21].

II. HAMILTONIAN

Our starting point is L qubits placed on the L vertices of graph G_L . The graph is specified by an $L \times L$ symmetric

*jtindall@flatironinstitute.org

Published by the American Physical Society under the terms of the [Creative Commons Attribution 4.0 International](https://creativecommons.org/licenses/by/4.0/) license. Further distribution of this work must maintain attribution to the author(s) and the published article's title, journal citation, and DOI.

adjacency matrix A_{G_L} with elements $A_{v,v'}$ which dictate the (weighted) connections between vertices (qubits) $v, v' \in [1, \dots, L], [1, \dots, L]$. The Hamiltonian reads

$$H(G_L) = \frac{1}{L} \sum_{\substack{v,v'=1 \\ v>v'}}^L A_{v,v'} \left(\sum_{\alpha=x,y,z} J^\alpha \hat{\sigma}_v^\alpha \hat{\sigma}_{v'}^\alpha \right) + \sum_{\substack{v \in V \\ \alpha=x,y,z}} h^\alpha \hat{\sigma}_v^\alpha, \tag{1}$$

with $J^\alpha, h^\alpha \in \mathbb{R}$ and $\hat{\sigma}_v^\alpha$ being the Pauli spin operator acting along the α spin axis on vertex v [22]. Our focus is on graphs where $0 \leq A_{v,v'} \leq 1$ and $\sum_{v,v'} A_{v,v'} \propto L^2$. When the graph is unweighted ($A_{v,v'} \in \{0, 1\}$), we refer to the graph as “dense” because the average coordination number diverges with system size. The factor of $\frac{1}{L}$ in $H(G_L)$ is necessary to ensure a finite, nontrivial energy density. A variety of well-known models—including the Curie-Weiss [23] and Lipkin-Meshkov-Glick [24,25] models—are contained within our Hamiltonian. The restriction $0 \leq A_{v,v'} \leq 1$ and the homogeneous nature of the field strengths, however, preclude our Hamiltonian from including disordered models such as spin-glass systems [26,27].

III. THEORY

In this work, by utilizing tools from graph theory and mean-field theory, we formulate an explicit, exact, continuous description of this system in thermal equilibrium in the thermodynamic limit. In order to describe our continuum formalism we must first introduce the concept of a graphon. This can be done by taking the vertices $v = 1, \dots, L$ of a graph G_L and performing the change in variables: $x = v/L \in [0, 1]$. We then define $W_{G_L}(x, y) : [0, 1]^2 \rightarrow [0, 1]$, a real symmetric stepped function over the unit square such that for a given $(x, y) \in I_v \times I_{v'}$, where $I_v = [(v-1)/L, v/L]$, $W_{G_L}(x, y) = A_{v,v'}$. With a well-defined metric for the similarity of two graphs, it can be shown that for certain sequences of graphs $(G_L)_{L \in \mathbb{N}}$ the limit $\lim_{L \rightarrow \infty} W_{G_L}(x, y)$ converges to a well-defined symmetric function $W(x, y)$ known as a “graphon” [17,18]. In the Appendixes we discuss these metrics in detail and provide theorems for the convergence of graph sequences under these metrics. Importantly, it is also possible to move in the opposite direction and, given a graphon $W(x, y)$, construct sequences of finite graphs whose limit is $W(x, y)$. These finite graphs can be constructed via one of two methods, “stochastic” or “weighted” sampling of $W(x, y)$, and we use G_L^S and G_L^W to refer to their respective realizations over the vertices $v = 1, \dots, L$. They can be constructed by defining the quantity

$$P_{v,v'} = L^2 \int_{I_v \times I_{v'}} W(x, y) dx dy, \quad I_v = [(v-1)/L, v/L]. \tag{2}$$

The adjacency matrix of the unweighted graph G_L^S is then defined by setting $A_{v,v'} = 1$ with probability $P_{v,v'}$ and $A_{v,v'} = 0$ otherwise. The adjacency matrix of the weighted graph G_L^W is defined by setting $A_{v,v'} = P_{v,v'}$. A given sequence

of such realizations is guaranteed to converge to the graphon $W(x, y)$ in the limit $L \rightarrow \infty$.¹

With the definition of the graphon in hand, the central result of this paper can be presented.

Theorem 1. Let $(G_L)_{L \in \mathbb{N}} = (G_1, G_2, \dots)$ be a sequence of finite-size graphs generated as stochastic or weighted realizations of the graphon $W(x, y)$. Then for a given inverse temperature $T = 1/\beta$ the macroscopic properties of the equilibrium states of the sequence of Hamiltonians $H(G_L)_{L \in \mathbb{N}} = (H(G_1), H(G_2), \dots)$ converge and are determined by the solution of the following coupled integral equations:

$$\lambda^\alpha(x) = -J^\alpha \int_0^1 \frac{W(x, y) \lambda^\alpha(y) \tanh[\beta \Lambda(y)]}{\Lambda(y)} dy + h^\alpha, \tag{3}$$

with $\alpha = x, y, z$; $\Lambda(x) = +\sqrt{[\lambda^x(x)]^2 + [\lambda^y(x)]^2 + [\lambda^z(x)]^2}$; and the three functions $\lambda^\alpha(x)$, with $\alpha \in \{x, y, z\}$, each being continuous, real valued, and defined over the domain $[0, 1]$.

In order to prove Theorem 1 and arrive at Eq. (3) we state the following intermediate theorem.

Theorem 2. Let $f(H) = -\frac{1}{L\beta} \ln\{\text{Tr}[\exp(-\beta H)]\}$ be the free energy density of a $d^L \times d^L$ many-body Hamiltonian, where $\beta \in \mathbb{R}_{\geq 0}$ and d is the dimension of the local Hilbert space. Let G_L^S and G_L^W be the stochastic and weighted realizations on L vertices of a graphon $W(x, y)$, respectively. For an arbitrary set of real, finite values for the parameters $\{J^x, J^y, J^z, h^x, h^y, h^z\}$ the following is true:

$$|f(H(G_L^S)) - f(H(G_L^W))| = O(L^{-1/2}), \tag{4}$$

which vanishes in the limit $L \rightarrow \infty$.

Theorem 2 is a significant generalization of Theorem 1 in Ref. [28], which proved this result solely for sequences of Erdős-Rényi graphs, which correspond to the constant graphon. The proof of Theorem 2 (which can be found in Appendix A) relies on more general statistical properties of random graphs.

With Theorem 2 in hand, Theorem 1 follows by (i) focusing strictly on the sequence $(G_L^W)_{L \in \mathbb{N}} = (G_1^W, G_2^W, \dots)$ of weighted finite realizations of $W(x, y)$, (ii) applying mean-field theory (which is exact here in the thermodynamic limit), and (iii) taking the continuum limit of the resulting equations by invoking the definition of the graphon. Appendix A contains full proofs of both Theorems 1 and 2.

If we can solve Eq. (3) for the functions $\{\lambda^x(x), \lambda^y(x), \lambda^z(x)\}$, then we have determined the equilibrium physics of the limit of the sequence $(H(G_1), H(G_2), \dots)$. The functions $\{\lambda^x(x), \lambda^y(x), \lambda^z(x)\}$ are a change in variables from the continuum limit of the spin degrees of freedom in the Hamiltonian. They directly encode the physical properties of the equilibrium state: the magnetization on site v in the thermodynamic limit is specified by $\langle \sigma^\alpha(x) \rangle$ with $x = \lim_{L \rightarrow \infty} \frac{v}{L}$ and is related to the

¹We point out that the Hamiltonian in Eq. (1) is invariant under $A_{G_L} \rightarrow A_{G_L} A, J^\alpha \rightarrow J^\alpha/c$. This degree of freedom on the graphon and the $P_{v,v'}$ is trivial as it does not affect its functional form — which is what governs the resulting equilibrium physics.

λ functions by

$$\langle \sigma^\alpha(x) \rangle = -\frac{\lambda^\alpha(x) \tanh[\Lambda(x)]}{\Lambda(x)}. \quad (5)$$

The total magnetization along a given spin direction is

$$M^\alpha = \lim_{L \rightarrow \infty} \frac{1}{L} \sum_{v=1}^L \langle \sigma_v^\alpha \rangle = -\int_0^1 \frac{\lambda^\alpha(x) \tanh[\Lambda(x)]}{\Lambda(x)} dx. \quad (6)$$

The validity of the mean-field approximation here means we can compute multipoint correlators as products of on-site expectation values.

How can we solve Eq. (3) and find $\{\lambda^x(x), \lambda^y(x), \lambda^z(x)\}$? In general there is no analytical solution, and we will be restricted to numerical methods. Nonetheless, there are certain cases where they can be solved analytically. Consider the case in which the graphon is degenerate, i.e., $W(x, y) = \sum_{i=1}^n f_i(x) f_i(y)$, where n is finite and $f_i(x) : [0, 1] \rightarrow [0, 1]$. Substitution into the above equation tells us $\lambda^\alpha(x) = \sum_{i=1}^n c_i^\alpha f_i(x)$, where c_i^α are real-valued coefficients which depend on the field strengths h^α , the couplings J^α , and the inverse temperature β but do not depend on x . These coefficients c_i^α are the solution of the set of $3n$ coupled equations which results from the substitution of $\lambda^\alpha(x) = \sum_{i=1}^n c_i^\alpha f_i(x)$ into Eq. (3). For a given set of J^α and h^α and a value of β we therefore have a closed form for $\lambda^\alpha(x)$ and various observables in the system. In our examples in the main text (further examples, including nondegenerate graphons, are considered in the Appendix C) we focus on $n = 1$ because such graphons can be manipulated to yield closed forms for the equilibrium properties of the system.

IV. CLASSICAL ISING MODEL

We first set $J^x = J^y = h^x = h^y = h^z = 0$ and $J^z = -1$, realizing the classical Ising model with zero field. Utilizing $\text{sgn}(z) \tanh(\beta|z|) = \tanh(z)$, our integral equations reduce to

$$\lambda^z(x) = \int_0^1 W(x, y) \tanh[\beta \lambda^z(y)] dy. \quad (7)$$

The \mathbb{Z}_2 spin-flip symmetry is encoded in the fact that if $\lambda^z(x)$ is a solution to the equation, then so is $-\lambda^z(x)$. Moreover, there is clearly always a trivial solution $\lambda^z(x) = 0 \forall x$ which corresponds to the disordered paramagnetic state with zero magnetization. Applying Banach's fixed-point theorem [29] to Eq. (7) tells us that, with certainty, when $\beta < \sup_{x \in [0, 1]} \int_0^1 W(x, y) dy$, this is the only solution. For larger values of β , however, a nontrivial solution exists which corresponds to a ferromagnetic phase. For instance, when $\beta \rightarrow \infty$, we have $\lambda^z(x) = \int_0^1 W(x, y) dx \neq 0 \forall x$. Thus, following this analysis, we know that $\lambda^z(x, \beta)$ cannot be smooth and continuous over $x \in [0, 1]$ and $\beta \in [0, \infty]$ and there must exist a finite-order transition between the ferromagnetic solution and the paramagnetic solution at some critical temperature. Our continuum description therefore allows us to prove the existence of a ferromagnetic-paramagnetic phase transition for the Ising model on *any* dense graph—with a corresponding analytical upper bound on this temperature. A similar argument can be applied to a number of the limits of Eq. (1).

Now let us treat some explicit examples. We first consider $W(x, y) = p$ whose stochastic realizations are $G_{\text{ER}}(p)$: the Erdős-Rényi graph over L vertices where each edge appears independently with probability p . Observe from Eq. (7) that in this case $\lambda^z(x) = \lambda^z = p \tanh(\beta \lambda^z)$ and is independent of x . Substituting this into Eq. (6) gives us the familiar self-consistent equation $M^z = \tanh(\beta p M^z)$ for the magnetization M^z of the classical Ising model under the mean-field approximation. The edge probability p re-scales the temperature in the all-to-all model and the randomness of the model has no effect on the macroscopic physics in the thermodynamic limit—a result which has been proven to be general for spin systems on Erdős-Rényi graphs [23,28].

We consider the more complex, separable graphon $W(x, y) = xy$, whose stochastic realizations dictate that each pair of spins v and v' interacts with strength 1 with probability (vv'/L^2) and strength 0 otherwise. One can also choose to directly interpret the deterministic realization of the graphon, in which each pair of spins interacts with a strength (vv'/L^2) . Both interpretations lead to the same physics in the thermodynamic limit—this follows directly from Theorem 2. From Eq. (7) we derive (see the Appendix B) $\sigma^z(x) = \tanh(\beta c x)$ and $M^z = \frac{\ln[\cosh(c)]}{c}$, where c is the real-valued solution of the equation

$$12c^2 - \pi^2 + 24c \ln(1 + e^{-2c}) - 12\text{PL}_2(-e^{-2c}) = \frac{24c^3}{\beta} \quad (8)$$

and PL_2 is the polylogarithm function of order 2. The critical inverse temperature β_c is $\beta_c = 3$: the supremum of the left-hand side of the above equation for $c \in [0, \infty]$.

In Fig. 1 we plot the total magnetization M^z and the local magnetization $\sigma^z(x)$ versus β based on our analytical solution. We also perform finite-size Monte Carlo numerics for M^z for increasing system size [by constructing stochastic realizations of $W(x, y)$] and demonstrate convergence to our analytical solution. We compare these results to the graphon $W(x, y) = \frac{1}{4}$. As the temperature increases, both systems undergo a second-order phase transition characterized by typical mean-field exponents. For the graphon $W(x, y) = xy$, however, the convergence to a fully ferromagnetic state at zero temperature is slower. This convergence can be determined analytically by expanding Eq. (8) for large β and substituting into $M^z = \frac{\ln[\cosh(c)]}{c}$, yielding $M^z = 1 - \frac{2 \ln(2)}{\beta}$. There is thus a direct linear convergence of the magnetization to unity with temperature $T = \frac{1}{\beta}$ versus the exponentially fast convergence associated with the homogeneous $W(x, y) = \text{const}$ case.

This slow convergence is a result of the “left boundary” of the system. In Fig. 1(b) we see that the local magnetization at small values of x , where the spin-spin couplings are very weak, is very small even deep in the ferromagnetic regime. This “boundary effect” means the $T = 0$ state has a finite magnetic susceptibility to changes in temperature, i.e., $\frac{dM^z}{dT} |_{T=0} = -2 \ln(2)$. In the homogeneous case we have $\frac{dM^z}{dT} |_{T=0} = 0$. While both systems are mean field in terms of their universal behavior, they exhibit very different physics in the ferromagnetic regime.

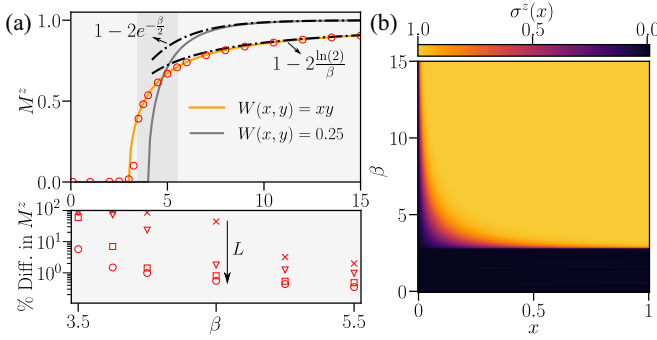


FIG. 1. Magnetization of the classical Ising model for the graphons: $W(x, y) = xy$ and $W(x, y) = \frac{1}{4}$. (a) Top: Total magnetization density M^z versus inverse temperature β for $L \rightarrow \infty$. Black dash-dotted lines give the asymptotic derived by taking the large- β limit of the respective closed-form equations. Red circles correspond to Monte Carlo simulations of finite, $L = 800$, randomly sampled graphons G_L^S derived from $W(x, y) = xy$. Bottom: Percentage difference in M^z for the exact result in the thermodynamic limit versus finite-size Monte Carlo simulations at several L (crosses show $L = 100$, triangles show $L = 200$, squares show $L = 400$, and circles show $L = 800$). For each β and L , 100 stochastic samples G_L^S are realized, and the data (both top and bottom plots) are averaged over these. Further details are provided in the Appendix. (b) On-site magnetization $\sigma^z(x)$ versus β and x for the graphon $W(x, y) = xy$ in the thermodynamic limit.

V. TRANSVERSE FIELD ISING MODEL

We now consider a quantum example: the transverse field Ising model. Our integral equation is [setting $J^x = J^y = h^y = h^z = 0$ and $h^x = -h, J^z = -1$ in Eq. (1)]

$$\lambda^z(x) = \int_0^1 \frac{W(x, y)\lambda^z(y) \tanh\{\beta\sqrt{h^2 + [\lambda^z(y)]^2}\}}{\sqrt{h^2 + [\lambda^z(y)]^2}} dy. \quad (9)$$

We focus on the ground state by taking the limit $\beta \rightarrow \infty$. We can again use Banach's fixed-point theorem here to prove the existence of a disordered-ordered phase transition with an upper bound of the critical field strength h_c given by the supremum of the marginal of the graphon.

We now consider some specific examples. First, taking the Erdős-Rényi graphon $W(x, y) = p$ straightforwardly yields the solution $M^z = \sqrt{1 - \frac{h^2}{p^2}}$, consistent with a rescaled transverse field Ising model with all-to-all coupling [28].

There are, however, other less trivial graphons for which an exact analytical solution for the ground state properties can be found. Consider the separable case $W(x, y) = \sqrt{xy}$. Some algebra on Eq. (9) (see the Appendix C) leads to $\langle \sigma^x(x) \rangle = \frac{h}{\sqrt{h^2 + g^2 x}}$ and $\langle \sigma^z(x) \rangle = -\frac{g\sqrt{x}}{\sqrt{h^2 + g^2 x}}$, with

$$g = \begin{cases} \frac{\sqrt{2}}{3} \sqrt{1 + (1 - 3h)\sqrt{1 + 6h}} & h < \frac{1}{2}, \\ 0 & \text{otherwise.} \end{cases} \quad (10)$$

Integrating the expression (see the Appendix C) for the transverse magnetization then gives the following closed form for

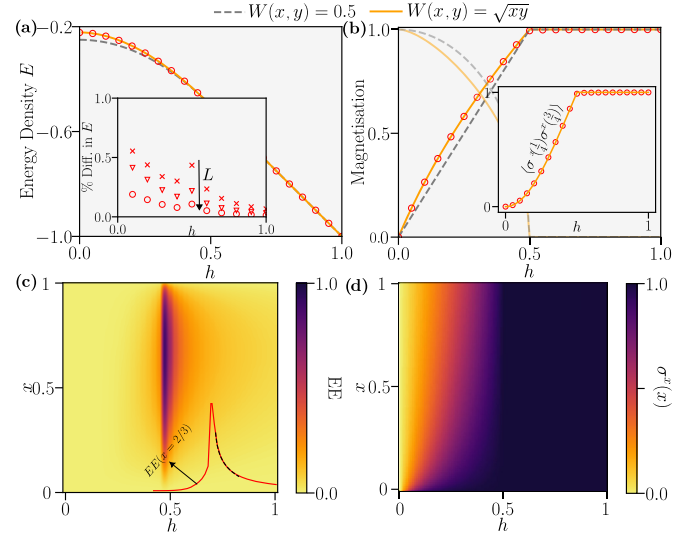


FIG. 2. Properties of the ground state of the transverse field Ising model on the graphon $W(x, y) = \sqrt{xy}$. Results for the constant graphon are included for reference. (a) Energy density versus transverse field strength h . The orange line represents the analytic solution in the thermodynamic limit. Markers represent numerical calculations averaged over 100 finite stochastic realizations of $W(x, y) = \sqrt{xy}$ on $L = 400$ sites. Inset: Percentage difference between the ground state energy calculated for $L = 100, 200,$ and 400 (crosses, triangles, and circles, respectively) site random-exchange realizations of $W(x, y)$ and the exact solution for $L \rightarrow \infty$. (b) Total transverse (unfaded) and longitudinal (faded) magnetization densities of the ground state. Inset: Two-point correlator $\langle \sigma^x(\frac{1}{4}) \sigma^x(\frac{3}{4}) \rangle$. (c) von Neumann entanglement entropy (EE) of $W(x, y) = \sqrt{xy}$ averaged over 100 stochastic realizations on $L = 400$ sites. The partition is between the first xL sites of the system and the remaining $(1 - x)L$ sites. The red curve corresponds to the entanglement entropy at $x = 2/3$ for $h = 0 \rightarrow 1$. The dotted black line is the fit $EE(x = 2/3) = -0.136 \log_2(h - 0.5) - 0.089$. (d) Analytical result for the on-site magnetization $\sigma^x(x)$ versus transverse field strength h and position x for the graphon $W(x, y) = \sqrt{xy}$.

the total transverse magnetization density:

$$M^x = \begin{cases} \frac{6h}{3h + \sqrt{2 + 9h^2 + (2 - 6h)\sqrt{1 + 6h}}} & h < \frac{1}{2}, \\ 1 & \text{otherwise.} \end{cases} \quad (11)$$

The total longitudinal magnetization density can also be obtained in closed form (see the Appendix C). Our methodology has yielded an analytic expression for the magnetization (in the thermodynamic limit) of the transverse field Ising model on a complex, highly inhomogeneous graph structure.

In Fig. 2 we plot these solutions alongside those for the constant graphon. The left boundary of the system, which has very weak z - z coupling, modifies the physics of the system and makes it more susceptible to the transverse field than the all-to-all case. The transverse field susceptibility versus site index x can be derived from Eq. (10), yielding $\lim_{h \rightarrow 0} \frac{d\langle \sigma^x(x) \rangle}{dh} = \delta(x)$, where $\delta(x)$ is the Dirac delta function. There is a singularity in the susceptibility on the left boundary of the system at zero field strength in the ferromagnetic regime. It is not present in the all-to-all model. Critical

exponents for the magnetizations at the phase transition can be found via expansion of the analytical results, and they are consistent with the mean-field universality class and equivalent for the two graphons.

In Fig. 2 we also provide finite-size simulations of the ground state on random-exchange realizations of $W(x, y)$ using density matrix renormalization group [30] calculations on a matrix product state ansatz. We reach system sizes on the order of ~ 100 spins, observing convergence to our analytical solution. We verify this convergence for local observables and nonlocal ones, where exact, analytical results can be obtained via the mean-field approximation.

Importantly, from these tensor network numerics we can go beyond mean-field theory and obtain the entanglement entropy of the ground state on a finite system—something currently inaccessible to our continuous formalism. This is nonzero and diverges logarithmically with the transverse field strength as criticality is approached: $h \rightarrow 0.5^-$. We also find the entanglement depends on only the ratio $x = N/L$, where N is the partition size. This scaling is reminiscent of the entanglement properties of the all-to-all transverse field Ising model [24]. Here we observe it in a heterogeneous dense graph system, suggesting a possible universal mechanism underpinning the scaling of entanglement entropy in these models.

VI. CONCLUSION

We have successfully utilized tools from graph theory to derive a set of integral equations which describes the physics of generic spin models with a large density of interactions in the thermodynamic limit—whether classical or quantum. Our formalism straightforwardly reproduces known results and, most importantly, can be used to uncover the equilibrium properties of more complex systems. We observed how inhomogeneity in the underlying graphs alters the magnetic properties of the system.

Our work opens a up a number of further avenues for future research. First, extending our formalism to describe the out-of-equilibrium dynamics of a spin system on a dense graph is a natural direction. While an analytical solution is known for the all-to-all case [$W(x, y) = 1$] in the Lipkin-Meshkov-Glick model (a model whose dynamics was recently realized on a quantum simulator [25]), our graph-theoretic approach could open up solutions for a whole range of dense graphs. The quantum fluctuations which deviate finite-size results from the mean-field case would be stronger there.

Second, graphon estimation is the process of estimating the continuous graphon $W(x, y)$ from which a given finite graph G could have been drawn [31–33]. Therefore, when studying spin models on a large, connected structure (the structure need not necessarily be dense; graphon estimation can be done for quasisparse graphs too [32,33]), one can estimate the graphon $W(x, y)$ and solve our equations to obtain an approximate solution to the equilibrium physics of the system.

ACKNOWLEDGMENTS

J.T. is grateful for ongoing support through the Flatiron Institute, a division of the Simons Foundation. A.S. acknowledges support from EPSRC Standard Research Studentship

(Doctoral Training Partnership), EP/T517811/1, and the Smith-Westlake Graduate Scholarship at St. Hugh’s College. We are grateful to S. Staton, D. Jaksch, D. Sels, and V. Oganesyan for fruitful discussions. Monte Carlo calculations were performed with code written solely by the authors, while density matrix renormalization group calculations were done with the help of the ITENSOR library [34].

APPENDIX A: PROOF OF THEOREMS 1 AND 2

We restate the Hamiltonian from the main text,

$$H(G_L) = \frac{1}{L} \sum_{\substack{v, v'=1 \\ v > v'}}^L A_{v, v'} \left(\sum_{\alpha} J^{\alpha} \hat{\sigma}_v^{\alpha} \hat{\sigma}_{v'}^{\alpha} \right) + \sum_{v \in V} h^{\alpha} \hat{\sigma}_v^{\alpha}, \quad (\text{A1})$$

where all definitions are retained and $\alpha = x, y, z$. We now prove Theorems 1 and 2 from the main text, which are restated below.

Theorem 1. Let $(G_L)_{L \in \mathbb{N}} = (G_1, G_2, \dots)$ be a sequence of finite-size graphs generated as stochastic or weighted realizations of the graphon $W(x, y)$. Then for a given inverse temperature $T = 1/\beta$ the macroscopic properties of the equilibrium states of the sequence of Hamiltonians $H(G_L)_{L \in \mathbb{N}} = (H(G_1), H(G_2), \dots)$ converge and are determined by the solution of the following coupled integral equations:

$$\lambda^{\alpha}(x) = -J^{\alpha} \int_0^1 \frac{W(x, y) \lambda^{\alpha}(y) \tanh[\beta \Lambda(y)]}{\Lambda(y)} dy + h^{\alpha}, \quad (\text{A2})$$

with $\alpha = x, y, z$; $\Lambda(x) = +\sqrt{[\lambda^x(x)]^2 + [\lambda^y(x)]^2 + [\lambda^z(x)]^2}$; and the three functions $\lambda^{\alpha}(x)$, with $\alpha \in \{x, y, z\}$, each being continuous, real valued, and defined over the domain $[0, 1]$.

Theorem 2. Let $f(H) = -\frac{1}{L\beta} \ln \{\text{Tr}[\exp(-\beta H)]\}$ be the free energy density of a $d^L \times d^L$ many-body Hamiltonian, where $\beta \in \mathbb{R}_{\geq 0}$ and d is the dimension of the local Hilbert space. Let G_L^S and G_L^W be the stochastic and weighted realizations on L vertices of a graphon $W(x, y)$ respectively. For an arbitrary set of real, finite values for the parameters $\{J^x, J^y, J^z, h^x, h^y, h^z\}$ the following is true:

$$|f(H(G_L^S)) - f(H(G_L^W))| = O(L^{-1/2}), \quad (\text{A3})$$

which vanishes in the limit $L \rightarrow \infty$.

We will first prove Theorem 1 by assuming that Theorem 2 is true. Then we will prove Theorem 2 to complete the proof.

We first perform a mean-field treatment of $H(G_L)$ for some arbitrary graph G_L with adjacency matrix elements $A_{v, v'}$ and take $L \rightarrow \infty$. Let $\hat{\sigma}_v^{\alpha} = \langle \hat{\sigma}_v^{\alpha} \rangle + \hat{\delta}_v^{\alpha}$, substitute it into the Hamiltonian, and ignore terms of order $\hat{\delta}^2$. The result is (up to a constant)

$$H(G_L) = \sum_v H_v = \sum_{v, \alpha} \hat{\sigma}_v^{\alpha} \left[\frac{1}{L} \left(\sum_{v'=1}^L A_{v, v'} J^{\alpha} \langle \hat{\sigma}_{v'}^{\alpha} \rangle \right) + h^{\alpha} \right]. \quad (\text{A4})$$

Within this mean-field approximation the equilibrium state of the system is given by

$$\rho(\beta) = \frac{\exp(-\beta H)}{\text{Tr}[\exp(-\beta H)]} = \bigotimes_{v=1}^L \frac{\exp(-\beta H_v)}{\text{Tr}[\exp(-\beta H_v)]} = \bigotimes_{v=1}^L \rho_v, \quad (\text{A5})$$

where the reduced density matrix on each site ρ_v is, explicitly (in the basis spanned by the eigenstates of σ^z), the following 2×2 matrix:

$$\rho_v = \frac{1}{2\lambda_v} \begin{pmatrix} \lambda_v - \lambda_v^z \tanh(\beta\lambda_v) & -(\lambda_v^x - i\lambda_v^y) \tanh(\beta\lambda_v) \\ -(\lambda_v^x + i\lambda_v^y) \tanh(\beta\lambda_v) & \lambda_v + \lambda_v^z \tanh(\beta\lambda_v) \end{pmatrix}, \quad (\text{A6})$$

where we have defined $\lambda_v = \sqrt{(\lambda_v^x)^2 + (\lambda_v^y)^2 + (\lambda_v^z)^2}$ and $\lambda_v^\alpha = \frac{1}{L} (\sum_{v'} A_{v,v'} J^\alpha \langle \hat{\sigma}_{v'}^\alpha \rangle) + h^\alpha$.

$$\lambda^\alpha(x) = - \left(\sum_{y=1/L, 2/L, \dots, L} \frac{J^\alpha L^2 \left(\int_{I_v \times I_{v'}} W(x, y) dx dy \right) \lambda^\alpha(x) \tanh[\beta \lambda(y)]}{\lambda(y)} \right) dx + h^\alpha. \quad (\text{A8})$$

Now we take $L \rightarrow \infty$, which implies $L^2 \int_{I_v \times I_{v'}} W(x, y) dx dy \rightarrow W(x, y)$, and the summation becomes an integral. We can then write down the coupled, continuous mean-field equations

$$\lambda^\alpha(x) = -J^\alpha \int_0^1 \frac{W(x, y) \lambda^\alpha(y) \tanh[\beta \Lambda(y)]}{\Lambda(y)} dy + h^\alpha, \quad (\text{A9})$$

with $\alpha = x, y, z$ and $\Lambda(x) = \sqrt{[\lambda^x(x)]^2 + [\lambda^y(x)]^2 + [\lambda^z(x)]^2}$. They govern our system in the thermodynamic limit of the sequence of graphs generated from the graphon $W(x, y)$. Although we explicitly used the weighted realization G_L^W of $W(x, y)$, Theorem 2 tells us that the equilibrium properties of the system that arise as the solution of Eq. (A9) are equivalent for both G_L^W and G_L^S as $L \rightarrow \infty$. Thus, these equations govern the properties of *any* sequence of finite graphs which converge to $W(x, y)$, not just weighted ones.

The equations in Eq. (A9) are coupled, nonlinear Fredholm integral equations with the graphon acting as the kernel. From the solution set $\{\lambda^x(x), \lambda^x(y), \lambda^y(z)\}$ to these equations we can obtain the on-site magnetizations via

$$\sigma^\alpha(x) = - \frac{\lambda^\alpha(x) \tanh[\beta \Lambda(x)]}{\Lambda(x)}, \quad (\text{A10})$$

and the total magnetization density is $M^\alpha = \int_0^1 \sigma(x) dx$.

In order to complete the proof of Theorem 1 we need to prove Theorem 2, which was assumed previously. We recall a lemma proven in Ref. [28] which will be helpful in completing the proof.

Lemma 1. Let $(A_L)_{L \in \mathbb{N}} = (A_1, A_2, \dots)$ and $(B_L)_{L \in \mathbb{N}} = (B_1, B_2, \dots)$ be two sequences of many-body Hermitian matrices. The matrices A_L and B_L in the sequence have size $d^L \times d^L$, with d being fixed and the dimension of the local Hilbert space. Let $D_L = A_L - B_L$ and λ_{Max}^D be the largest (in terms of the absolute value) eigenvalue of D_L . If $|\lambda_{\text{Max}}^D|$

By taking the expectation values $\langle \sigma_v^\alpha \rangle$ associated with ρ_v we find the λ_v^α variables must obey the following self-consistency relation:

$$\lambda_v^\alpha = - \frac{1}{L} \left(\sum_{v'=1}^L \frac{J^\alpha A_{v,v'} \lambda_{v'}^\alpha \tanh(\beta \lambda_{v'})}{\lambda_v} \right) + h^\alpha, \quad (\text{A7})$$

with $v = 1, \dots, L$ and $\alpha = x, y, z$. The set of values $\{\lambda_v^\alpha\}$, with $v = 1, \dots, L$ and $\alpha = x, y, z$, which solves the $3L$ nonlinear equations described by Eq. (A7), thus fully characterizes the mean-field equilibrium state associated with H .

Now we wish to take the continuum limit of Eq. (A7). First, we define the following: $x = v/L$, $dx = 1/L$, $\lambda_v^\alpha = \lambda^\alpha(x)$, and $\lambda_v = \lambda(x)$. We assume that the adjacency matrix has been generated as a weighted realization of some graphon $W(x, y)$, i.e., $A_{v,v'} = L^2 \int_{I_v \times I_{v'}} W(x, y) dx dy$, $I_v = [(v-1)/L, v/L]$. Substituting this into Eq. (A7) gives us

$= O(L^\kappa)$, then $|f(A_L) - f(B_L)| = O(L^{\kappa-1})$, which vanishes for $\kappa < 1$ as $L \rightarrow \infty$.

We begin by defining the following operator:

$$D_L := H(G_L^S) - H(G_L^W) = \sum_{\alpha=x,y,z} D_L^\alpha = \sum_{\alpha=x,y,z} \frac{1}{L} \left(\sum_{\substack{i,j=1 \\ i < j}}^L A_{ij}^S \hat{\sigma}_i^\alpha \hat{\sigma}_j^\alpha - \sum_{\substack{i,j=1 \\ i < j}}^L A_{ij}^W \hat{\sigma}_i^\alpha \hat{\sigma}_j^\alpha \right), \quad (\text{A11})$$

where A_{ij}^S are the matrix elements of G_L^S and A_{ij}^W are the matrix elements of G_L^W , which are finite stochastic and weighted realizations of some graphon $W(x, y)$.

We proceed to evaluate the eigenvalues of the operator D_L^α . As such, consider its eigenstates $|\sigma_1^\alpha, \dots, \sigma_L^\alpha\rangle$, where $\hat{\sigma}_i^\alpha |\sigma_1^\alpha, \dots, \sigma_L^\alpha\rangle = \mu_i |\sigma_1^\alpha, \dots, \sigma_L^\alpha\rangle$, with $\mu_i = \pm 1$, depending on whether the i th spin is pointing ‘‘up’’ or ‘‘down’’ in that basis. We define $\mu_{ij} := \mu_i \mu_j$ and consider the eigenvalue

$$\langle \sigma_1^\alpha, \dots, \sigma_L^\alpha | D_L^\alpha | \sigma_1^\alpha, \dots, \sigma_L^\alpha \rangle = \frac{1}{L} \left(\sum_{\substack{i,j=1 \\ i < j}}^L A_{ij}^S \mu_{ij} - \sum_{\substack{i,j=1 \\ i < j}}^L A_{ij}^W \mu_{ij} \right). \quad (\text{A12})$$

We proceed to show that, independent of the eigenstate $|\sigma_1^\alpha, \dots, \sigma_L^\alpha\rangle$, this eigenvalue grows, at most, as $L^{1/2}$ in the large- L limit. From there we can invoke Weyl’s inequality to show that the eigenvalues of D_L grow asymptotically as $L^{1/2}$ and subsequently invoke Lemma 1 to complete the proof of Theorem 1.

To prove the $L^{1/2}$ growth of Eq. (A12), we begin with the Hoeffding inequality. It states that for independent random variables Y_1, \dots, Y_n for which $a_i \leq Y_i \leq b_i$, the sum S_n

$:= Y_1 + Y_2 + \dots + Y_n$ is bounded as

$$P(|S_n - \mathbb{E}(S_n)| \geq t) \leq 2 \exp\left(-\frac{2t^2}{\sum_{i=1}^n (a_i - b_i)^2}\right), \quad (\text{A13})$$

with the factor of 2 stemming from the fact we have incorporated both the upper and lower Hoeffding bounds together. We will apply this bound to Eq. (A12).

Let us construct the set $X := \{X_{ij}\}$, which consists of the $\frac{L(L-1)}{2}$ random variables $X_{ij} := A_{ij}^S \mu_{ij}$ (we have $i, j = 1, \dots, L$ and $i > j$). Observe that since $A_{ij}^S \in \{0, 1\}$ (the graph G_L^S is simple) and μ_{ij} is either 1 or -1 , we have $-1 \leq X_{ij} \leq 1$. Also, $\mathbb{E}(X_{ij}) = \mathbb{E}(A_{ij}^S) \mu_{ij} = A_{ij}^W \mu_{ij}$, where $\mathbb{E}(A_{ij}^S)$ denotes the expected value. In our case, however, all of the X_{ij} quantities are not independent—the sign of X_{ij} is determined from the sign of X_{ik} and X_{kj} . This can be dealt with by applying the Hoeffding bound to the X_{ij} 's with positive and negative signs separately.

A given eigenvector $|\sigma_1^\alpha, \dots, \sigma_L^\alpha\rangle$ will consist of a number of spins pointing up ($\sigma_i = +1$), with the remainder pointing down ($\sigma_i = -1$). Define $M = \sum_{k=1}^L \sigma_k$; then it can be checked that of the $\frac{L(L-1)}{2}$ parameters μ_{ij} , $\frac{L^2+M^2-2L}{4}$ are positive, and $\frac{L^2-M^2}{4}$ are negative. We therefore partition the set $X := \{X_{ij}\}$ into two sets as follows:

$$\begin{aligned} x^A &:= \{X_{ij} | \mu_{ij} = 1\}, \\ x^B &:= \{X_{ij} | \mu_{ij} = -1\}. \end{aligned}$$

We would like also to keep track of the values $A_{ij}^W \mu_{ij}$, so we partition the set $\{\mu_{ij} A_{ij}^W\}$ into

$$\begin{aligned} \bar{x}^A &:= \{\mu_{ij} A_{ij}^W | \mu_{ij} = 1\}, \\ \bar{x}^B &:= \{\mu_{ij} A_{ij}^W | \mu_{ij} = -1\}. \end{aligned}$$

We can now invoke the Hoeffding bound on each set separately since each set now consists of independent random variables. We have two sums on which to invoke the bound: $S^A := \sum_{l=1}^{\frac{M^2+L^2-2L}{4}} x_l^A$ and $S^B := \sum_{l=1}^{\frac{L^2-M^2}{4}} x_l^B$, where we use x_l^A and x_l^B to refer to elements from x^A and x^B , respectively. Likewise, we will use \bar{x}_l^A and \bar{x}_l^B to refer to individual elements of \bar{x}^A and \bar{x}^B , respectively. Then we observe that, due to $\mathbb{E}(X_{ij}) = A_{ij}^W \mu_{ij}$, we have $\mathbb{E}(S^A) = \sum_{l=1}^{\frac{M^2+L^2-2L}{4}} \bar{x}_l^A$ and $\mathbb{E}(S^B) = \sum_{l=1}^{\frac{L^2-M^2}{4}} \bar{x}_l^B$.

Equation (A13) then gives two bounds:

$$\begin{aligned} P(|S^A - \mathbb{E}(S^A)| \geq t_1) &\leq 2 \exp\left(\frac{-2t_1^2}{L^2 + M^2 - 2L}\right), \\ P(|S^B - \mathbb{E}(S^B)| \geq t_2) &\leq 2 \exp\left(\frac{-2t_2^2}{L^2 - M^2}\right). \end{aligned}$$

We combine these bounds to obtain

$$\begin{aligned} P\left(\left|\sum_{\substack{i,j=1 \\ i < j}}^L \mu_{ij} A_{ij}^S - \sum_{\substack{i,j=1 \\ i < j}}^L \mu_{ij} A_{ij}^W\right| \geq t_1 + t_2\right) \\ \leq 4 \exp\left(\frac{-2t_1^2}{L^2 + M^2 - 2L}\right) \exp\left(\frac{-2t_2^2}{L^2 - M^2}\right). \quad (\text{A14}) \end{aligned}$$

Since we fixed the magnetization M of the eigenstate in deriving the above bound, we should take the union bound over $\binom{L}{\frac{1}{2}(L+M)}$ eigenstates with magnetization M . We will denote an eigenstate with magnetization M as $|\sigma_M\rangle$, resulting in the new bound

$$\begin{aligned} \bigcup_{|\sigma_M\rangle} P\left(\left|\sum_{\substack{i,j=1 \\ i < j}}^L \mu_{ij} A_{ij}^S - \sum_{\substack{i,j=1 \\ i < j}}^L \mu_{ij} A_{ij}^W\right| \geq t_1 + t_2\right) \\ \leq 4 \binom{L}{\frac{1}{2}(L+M)} \exp\left(\frac{-2t_1^2}{L^2 + M^2 - 2L}\right) \exp\left(\frac{-2t_2^2}{L^2 - M^2}\right). \quad (\text{A15}) \end{aligned}$$

Now we observe that the following is true:

$$\begin{aligned} \binom{L}{\frac{1}{2}(L+M)} \exp\left(\frac{-2t_1^2}{L^2 + M^2 - 2L}\right) \exp\left(\frac{-2t_2^2}{L^2 - M^2}\right) \\ \leq \binom{L}{\frac{L}{2}} \exp\left(-\frac{t_1^2 + t_2^2}{L^2}\right), \quad (\text{A16}) \end{aligned}$$

where $L \in \mathbb{N}$, $|M| \leq L$ and $t_1, t_2 \in \mathbb{R}^+$.

This leads us to the following:

$$\begin{aligned} \bigcup_M \bigcup_{|\sigma_M\rangle} P\left(\left|\sum_{\substack{i,j=1 \\ i < j}}^L \mu_{ij} A_{ij}^S - \sum_{\substack{i,j=1 \\ i < j}}^L \mu_{ij} A_{ij}^W\right| \geq t_1 + t_2\right) \\ \leq 4(L+1) \binom{L}{\frac{L}{2}} \exp\left(-\frac{t_1^2 + t_2^2}{L^2}\right), \quad (\text{A17}) \end{aligned}$$

where the union bound has again been used. Now we observe that if $t_1 + t_2 = O(L^\gamma)$, then $t_1^2 + t_2^2 = O(L^{2\gamma})$, where $\gamma \in \mathbb{R}$.

Using the fact that $\binom{L}{\frac{L}{2}} \sim \sqrt{\frac{2}{L\pi}} 2^L$ for large L and also using $2^L = e^{L \ln(2)}$, we then arrive at

$$\begin{aligned} \bigcup_M \bigcup_{|\sigma_M\rangle} P\left(\left|\sum_{\substack{i,j=1 \\ i < j}}^L \mu_{ij} A_{ij}^S - \sum_{\substack{i,j=1 \\ i < j}}^L \mu_{ij} A_{ij}^W\right| \geq O(L^\gamma)\right) \\ \leq 2(L+1) \sqrt{\frac{2}{L\pi}} \exp[L \ln(2) - O(L^{2\gamma-2})], \quad (\text{A18}) \end{aligned}$$

which vanishes unless $\gamma \leq \frac{3}{2}$. This leads us to

$$\langle \sigma_1^\alpha, \dots, \sigma_L^\alpha | D_L^\alpha | \sigma_1^\alpha, \dots, \sigma_L^\alpha \rangle = O(L^{\frac{3}{2}}) \quad \forall M, |\sigma\rangle. \quad (\text{A19})$$

Now from Weyl's inequality we know that the eigenvalues of the operator $D_L = H(G_L^S) - H(G_L^W)$ are therefore bounded as $O(L^{1/2})$. From here we can invoke Lemma 1 with $\kappa = 1/2$, and Theorem 2 is proven.

APPENDIX B: ANALYTICAL SOLUTION OF THE CLASSICAL ISING MODEL FOR $W(x, y) = xy$

We wish to solve Eq. (7) with $W(x, y) = xy$, i.e., identify the function $\lambda^z(x)$ which solves

$$\lambda^z(x) = \int_0^1 xy \tanh[\beta \lambda^z(y)] dy. \quad (\text{B1})$$

We start by observing that $\lambda^z(x) = f(\beta)x$, where $f(\beta)$ is a real-valued function of β that is independent of x . Substituting this into Eq. (B1) and defining $c = \beta f(\beta)$ give us

$$\frac{c}{\beta} = \int_0^1 y \tanh(cy) dy. \tag{B2}$$

We can perform the integration here analytically. First, we perform integration by parts and expand into exponentials:

$$\begin{aligned} \int_0^1 y \tanh(cy) dy &= \frac{1}{c^2} \left(\left[\frac{1}{2} y^2 \tanh(cy) \right]_0^c - \frac{1}{2} \int_0^c y^2 \operatorname{sech}^2(y) dy \right) \\ &= \frac{1}{c^2} \left(\frac{c^2 \tanh(c^2)}{2} - \int_0^c \frac{2y^2 e^{-2y}}{(1 + e^{-2y})^2} dy \right). \end{aligned} \tag{B3}$$

Now the integral on the right-hand side can be dealt with by observing that $\frac{e^{-2y}}{(1+e^{-2y})^2} = \sum_{n=1}^{\infty} (-1)^{n-1} n e^{-2ny}$, giving us

$$\begin{aligned} c^2 \int_0^1 y \tanh(cy) dy &= \frac{c^2 \tanh(c^2)}{2} - \sum_{n=1}^{\infty} (-1)^{n-1} n \int_0^c 2y^2 e^{-2ny} dy \\ &= \frac{c^2 \tanh(c^2)}{2} - \sum_{n=1}^{\infty} \frac{(-1)^n \{1 + e^{-2cn} [1 + 2cn(1 + cn)]\}}{2n^2}. \end{aligned} \tag{B4}$$

We can evaluate the series by splitting up the numerator and using known results,

$$\begin{aligned} c^2 \int_0^1 y \tanh(cy) dy &= \frac{1}{2} - \frac{\pi^2}{24c^2} + \frac{1}{c} \ln(1 + e^{-2c}) \\ &\quad - \frac{1}{2c^2} \operatorname{PL}_2(-e^{-2c}). \end{aligned} \tag{B5}$$

We can then use this result to reduce Eq. (B1) to Eq. (8) from the main text:

$$\frac{1}{\beta} = \frac{1}{24c^3} [12c^2 - \pi^2 + 24c \ln(1 + e^{-2c}) - 12 \operatorname{PL}_2(-e^{-2c})]. \tag{B6}$$

Additionally, it is straightforward to observe that $M^z = \int_0^1 \sigma^z(x) dx = \int_0^1 \tanh(cx) dx = \frac{\ln[\cosh(c)]}{c}$.

APPENDIX C: ANALYTICAL SOLUTION OF THE GROUND STATE OF THE TRANSVERSE FIELD ISING MODEL FOR $W(x, y) = \sqrt{xy}$

We wish to solve Eq. (9) in the main text with $W(x, y) = \sqrt{xy}$ and $\beta = \infty$, i.e.,

$$\lambda^z(x) = \sqrt{x} \int_0^1 \frac{\sqrt{y} \lambda^z(y)}{\sqrt{h^2 + [\lambda^z(y)]^2}} dy, \tag{C1}$$

again observing that this implies $\lambda^z(x) = \sqrt{x}g(h)$, where $g(h)$ is some real-valued function of h , giving

$$\int_0^1 \frac{y}{\sqrt{h^2 + g^2(h)y}} dy = 1, \tag{C2}$$

which we can solve for $g(h)$ [we restrict h and $g(h)$ to be positive real without loss of generality] using a series of substitutions. This yields

$$\frac{2[2h^3 - 2h^2\sqrt{h^2 + g^2(h)} + g^2(h)\sqrt{h^2 + g^2(h)}]}{3g^4(h)} = 1, \tag{C3}$$

which has the solution

$$g(h) = \begin{cases} \frac{\sqrt{2}}{3} \sqrt{1 + (1 - 3h)\sqrt{1 + 6h}} & h < \frac{1}{2}, \\ 0 & \text{otherwise,} \end{cases} \tag{C4}$$

as in the main text. The transverse and longitudinal magnetizations are determined by the integrals $M^x = \int_0^1 \frac{h}{\sqrt{h^2 + g^2(h)x}} dx$ and $M^z = -\int_0^1 \frac{g(h)\sqrt{x}}{\sqrt{h^2 + g^2(h)x}} dx$, respectively. The first, by direct integration, yields Eq. (11) in the main text. The second can be done by an extensive series of trigonometric substitutions and results in the following closed-form expression:

$$M^z(x) = \begin{cases} \frac{(1+s)[2\sqrt{(1-s)(4+18h^2-4s)} - 9h^2[2\ln(3)+2\ln(h)-2\ln(-\sqrt{2-2s}+\sqrt{2+9h^2-2s})]]}{108h^2(-1+2h)} & \\ 0 & \text{otherwise,} \end{cases} \tag{C5}$$

where $s = (-1 + 3h)\sqrt{1 + 6h}$.

APPENDIX D: FURTHER EXAMPLE GRAPHONS

In this Appendix we consider further graphons which were not treated in the main text but frequently appear in the literature on graphons.

1. Stochastic block models

The stochastic block graphon is typically utilized in statistical analysis of networks because they are useful in uncovering clustering in networks [35]. The graphon can be expressed as

$$W(x, y) = \begin{cases} p_{11} & \text{if } (x, y) \in X_1 \times X_1, \\ p_{12} & \text{if } (x, y) \in X_1 \times X_2, \\ \dots & \\ p_{kk} & \text{if } (x, y) \in X_k \times X_k, \end{cases} \quad (\text{D1})$$

with $p_{ij} = p_{ji}$ and X_i specifying disjoint subdomains of $[0,1]$ such that $\cup_{i=1}^k X_i = [0, 1]$. We write ΔX_i to indicate the width of the interval X_i . The continuous mean-field equations then take on the following form:

$$\lambda^\alpha(x) = -J^\alpha \sum_{j=1}^k \int_{X_j} \frac{p_{ij} \lambda^\alpha(y) \tanh\{\beta \sqrt{[\lambda^x(y)]^2 + [\lambda^y(y)]^2 + [\lambda^z(y)]^2}\}}{\sqrt{[\lambda^x(y)]^2 + [\lambda^y(y)]^2 + [\lambda^z(y)]^2}} dy + h^\alpha \quad \forall x \in X_i. \quad (\text{D2})$$

Observe that we can immediately infer from this that $\lambda^\alpha(x)$ is constant across each of the domains X_i . We can thus define $\lambda_i^\alpha = \lambda^\alpha(x) \forall x \in X_i$ and reduce Eq. (D3) to

$$\lambda_i^\alpha = -J^\alpha \sum_{j=1}^k \Delta X_j \frac{p_{ij} \lambda_j^\alpha \tanh[\beta \sqrt{(\lambda_j^x)^2 + (\lambda_j^y)^2 + (\lambda_j^z)^2}]}{\sqrt{(\lambda_j^x)^2 + (\lambda_j^y)^2 + (\lambda_j^z)^2}} + h^\alpha, \quad (\text{D3})$$

a series of equations which becomes increasingly complicated to solve as the number of clusters increases. In the case of a single cluster we recover the case of an Erdős-Rényi graph.

2. Growing uniform attachment

The growing uniform attachment graphon is given by $W(x, y) = 1 - \max(x, y)$ [36]. The graphs which are finite realizations of this graphon will consist of nodes in which the average connectivity of a node varies uniformly across the graph. Such graphs are therefore highly inhomogeneous in their average vertex connectivity. Substituting $W(x, y) = 1 - \max(x, y)$ into Eq. (A9) and differentiating the left- and right-hand sides twice with respect to x lead us to the following coupled second-order with Ordinary Differential Equations (ODE's):

$$\frac{d^2 \lambda^\alpha(x)}{dx^2} = J^\alpha \frac{\lambda^\alpha(x) \tanh[\beta \sqrt{\lambda^x(x)^2 + \lambda^y(x)^2 + \lambda^z(x)^2}]}{\sqrt{\lambda^x(x)^2 + \lambda^y(x)^2 + \lambda^z(x)^2}}, \quad (\text{D4})$$

with $\alpha = x, y, z$, boundary conditions $\lambda^\alpha(1) = 0$, and $\frac{d\lambda^\alpha(x)}{dx}|_{x=0} = 0 \forall \alpha$.

3. Maximally irregular graph

The maximally irregular graph is the finite connected graph in which each site (other than one pair) has a different coordination number from all the others [28]. Taking the thermodynamic limit of the adjacency matrix results in the graphon

$$W(x, y) = \begin{cases} 1 & x + y \leq 1, \\ 0 & \text{otherwise,} \end{cases} \quad (\text{D5})$$

and the integral equations in Eq. (A9) reduce (upon differentiation) to the following three coupled first-order ODEs:

$$\frac{d\lambda^\alpha(x)}{dx} = -J^\alpha \frac{\lambda^\alpha(1-x) \tanh\{\beta \sqrt{[\lambda^x(1-x)]^2 + [\lambda^y(1-x)]^2 + [\lambda^z(1-x)]^2}\}}{\sqrt{[\lambda^x(1-x)]^2 + [\lambda^y(1-x)]^2 + [\lambda^z(1-x)]^2}}, \quad \alpha = x, y, z, \quad (\text{D6})$$

with boundary conditions $\lambda^\alpha(1) = 0 \forall \alpha$. Such equations are known as functional differential equations and have been studied extensively in both mathematics and the applied sciences [37].

APPENDIX E: NUMERICAL DETAILS

1. Classical Ising model

For the finite-size data plotted in Fig. 1 of the main text we used Monte Carlo simulations. Specifically, for a given L we drew a finite random-exchange realization of the graphon $W(x, y) = xy$, and for a given temperature β we utilized the Metropolis-Hastings algorithm to generate $N_{\text{Samples}} = 5000$ for the magnetization density M^z . We used a Markov chain

length of 250 between each sample and threw away the first 1000 samples. For each L we took 100 stochastic realizations of the graphon $W(x, y)$ and averaged our results over them. There are thus two sources of statistical error in our simulations: the error from sampling a finite number of stochastic realizations and the error from taking a finite number of Monte Carlo samples. In Fig. 3 we plot the standard error of the mean from both of these sources; the values are negligible in comparison to the scale ($0 \rightarrow 1$) of Fig. 1 in the main text.

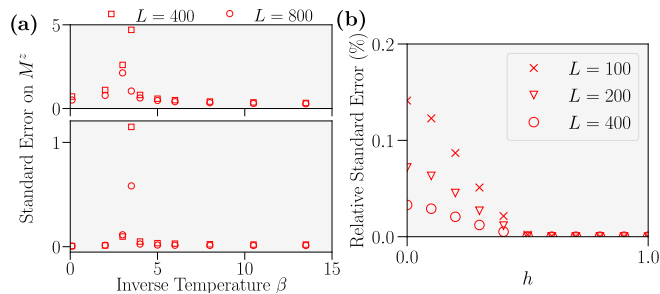


FIG. 3. (a) Standard error of the mean for the Monte Carlo calculations of M^z for the classical Ising model on stochastic finite-size realizations of $W(x, y) = xy$. The top plot is the standard error of the mean from 5000 Monte Carlo samples of M^z at a given β and L . Data points are averaged over 100 stochastic realizations of $W(x, y)$. The bottom plot is the standard error of the mean from the 100 stochastic realizations of $W(x, y)$ averaged over the 5000 samples taken for each realization. (b) Relative standard error of the mean (standard error of the mean as a percentage of the mean) for the ground state energy of the transverse field Ising model calculated via DMRG. Standard error is that originating from the 100 stochastic realizations of $W(x, y) = \sqrt{xy}$ at a given h and system size L .

2. Transverse Ising model

For the data plotted in Fig. 2 of the main text we used the density matrix renormalization group (DMRG) algorithm to find the ground state of the transverse field Ising model. For a given L we drew a finite stochastic realization of the graphon $W(x, y) = \sqrt{xy}$. Then, for a given field strength h we took a random matrix product state with a small bond dimension χ and successively performed DMRG sweeps, letting the bond dimension double every fourth sweep until the energy converged to within 0.1% of that for the previous bond dimension. There is thus only one source of statistical error in this simulation: the error from sampling a finite number (100) of stochastic realizations. In Fig. 3 we plot this error as a percentage and observe that it is on the order of 0.1%. The ordering of the sites (from left to right) of the matrix product state was taken to be identical to the ordering $v = 1, \dots, L$ of the sites of the graph.

APPENDIX F: THE GRAPHON AS THE LIMIT OBJECT OF DENSE GRAPH SEQUENCES

We provide mathematical details on how the graphon W is the limit object of a sequence of dense graphs $(G_n)_{n \in \mathbb{N}}$, where n is the number of vertices. This Appendix closely follows Ref. [38], although the theory on graph limits was first developed in Ref. [17]. The interested reader should consult either of those for more detail.

Consider two simple graphs F and G , where we define the number of vertices of F to be k and that of G to be n . A homomorphism from F to G is a map which preserves edges. This means that given an edge $(i, j) \in E(F)$ [here $E(F)$ is the edge set of F] and a homomorphism h , there is always an edge $(h(i), h(j)) \in E(G)$, the set of edges of G . Let $\text{hom}(F, G)$ indicate the number of homomorphisms from F into G . The

homomorphism density $t(F, G)$ is then defined as

$$t(F, G) = \frac{\text{hom}(F, G)}{n^k}. \quad (\text{F1})$$

The homomorphism density is the probability of a random map from graph F to graph G being a homomorphism since n^k is the total number of maps from a graph with k vertices to a graph with n vertices.

Suppose that, instead, we are given a graphon, such as W_G , the stepped graphon corresponding to graph G , which is defined as $W_G(x, y) = A_{v, v'}$ for $(x, y) \in [(v-1)/n, v/n] \times [(v'-1)/n, v'/n]$ (with A being the adjacency matrix of G). In this case, the homomorphism density is defined as

$$t(F, W_G) = \int_{[0,1]^k} \prod_{(i,j) \in E(F)} W(x_i, x_j) \prod_{i \in 1:k} dx_i. \quad (\text{F2})$$

Here the same definition holds for any arbitrary graphon W .

The homomorphism density with reference to a finite graph F indicates the relative likelihood of graph G or, more generally, graphon W containing an instance of F inside of it. If two graphs or graphons have similar homomorphism densities for *all* simple graphs F , then those graphs are similar. The definition of convergence of a sequence of graphs hinges precisely on this concept.

Definition 1. Convergent graph sequence. A sequence (G_n) of simple graphs with $V(G_n) \rightarrow \infty$ as $n \rightarrow \infty$ converges if the subgraph densities $t(F, G_n)$ converge for all simple graphs F .

The above definition allows us to precisely define in what sense W can be considered a limit object.

Theorem 3. Let (G_n) be a sequence of simple graphs with $V(G_n) \rightarrow \infty$. If (G_n) converges, a graphon W exists such that $t(F, G_n) \rightarrow t(F, W)$ for all simple graphs F [38].

Theorem 3 tells us that if the sequence (G_n) converges, then some limit object—the graphon—exists which captures the limiting homomorphism density counts of the sequence of graphs for *all* simple graphs.

There is a second, equivalent definition of convergence which allows us to define W as an appropriate limit of a sequence of dense graphs. This definition utilizes the cut distance of two graphs.

Definition 2. Cut distance. Given two graphons W and W' , define the cut distance between them to be

$$\begin{aligned} \delta_{\square}(W, W') \\ := \inf_{\phi, \psi} \sup_{S, T} \left| \int_{S \times T} [W(\phi(x), \phi(y)) - W'(\psi(x), \psi(y))] \right|, \end{aligned} \quad (\text{F3})$$

where the infimum is taken over all vertex relabelings ϕ of W and ψ of W' . The supremum is taken over all measurable subsets S and T of $[0, 1]$.

The cut distance is a metric on the space of graphons (up to weak isomorphism). It maximizes the difference between the integral of the two graphons on measurable intervals S and T , which together form a box $S \times T$. This step can be thought of as maximizing the difference in edges between those vertices contained in $S \times T$. The infimum is then taken on that chosen interval over all measure-preserving maps in order to ensure

that the cut distance is zero for weakly isomorphic graphons. The following theorem can then be proven from the above definitions.

Theorem 4. Given a sequence (G_n) of simple graphs with $|V(G_n)| \rightarrow \infty$ as $n \rightarrow \infty$, the sequence is said to converge to graphon W if $\delta_{\square}(W_{G_n}, W) \rightarrow 0$ as $n \rightarrow \infty$ [38].

This theorem provides an alternative definition for the graphon as a limit object. In this definition, we envisage instead the pixelated adjacency matrix of the sequence of

simple graphs G_n approaching (via the cut distance) that of the limit object W .

Importantly, the above definitions and theorems can be generalized to sequences of weighted graphs by requiring the graphs to have uniformly bounded edge weights. Moreover, we emphasize that these limits make sense only for sequences of *dense* graphs because it can be shown that sparse graph sequences always have as their limit the graphon $W(x, y) = 0$ for all x and y .

-
- [1] M. D. F. Shirley and S. P. Rushton, The impacts of network topology on disease spread, *Ecol. Complexity* **2**, 287 (2005).
- [2] S. Lozano, L. Buzna, and A. Díaz-Guilera, Role of network topology in the synchronization of power systems, *Eur. Phys. J. B* **85**, 231 (2012).
- [3] X. F. Wang, Complex networks: Topology, dynamics and synchronization, *Int. J. Bifurcation Chaos* **12**, 885 (2002).
- [4] A. Zakharova, M. Kapeller, and E. Schöll, Chimera death: Symmetry breaking in dynamical networks, *Phys. Rev. Lett.* **112**, 154101 (2014).
- [5] F. A. Rodrigues, T. K. D. Peron, P. Ji, and J. Kurths, The Kuramoto model in complex networks, *Phys. Rep.* **610**, 1 (2016).
- [6] K. Takano, K. Kubo, and H. Sakamoto, Ground states with cluster structures in a frustrated Heisenberg chain, *J. Phys.: Condens. Matter* **8**, 6405 (1996).
- [7] P. R. A. Campos, V. M. de Oliveira, and F. G. Brady Moreira, Small-world effects in the majority-vote model, *Phys. Rev. E* **67**, 026104 (2003).
- [8] A. Georges, G. Kotliar, W. Krauth, and M. J. Rozenberg, Dynamical mean-field theory of strongly correlated fermion systems and the limit of infinite dimensions, *Rev. Mod. Phys.* **68**, 13 (1996).
- [9] G. Kotliar, S. Y. Savrasov, K. Haule, V. S. Oudovenko, O. Parcollet, and C. A. Marianetti, Electronic structure calculations with dynamical mean-field theory, *Rev. Mod. Phys.* **78**, 865 (2006).
- [10] A. I. Lichtenstein, M. I. Katsnelson, and G. Kotliar, Finite-temperature magnetism of transition metals: An *ab initio* dynamical mean-field theory, *Phys. Rev. Lett.* **87**, 067205 (2001).
- [11] P. A. Pearce, Mean-field bounds on the magnetization for ferromagnetic spin models, *J. Stat. Phys.* **25**, 309 (1981).
- [12] D. Yamamoto, Correlated cluster mean-field theory for spin systems, *Phys. Rev. B* **79**, 144427 (2009).
- [13] F. L. Metz and T. Peron, Mean-field theory of vector spin models on networks with arbitrary degree distributions, *J. Phys.: Complexity* **3**, 015008 (2022).
- [14] F. G. S. L. Brandão and A. W. Harrow, Product-state approximations to quantum states, *Commun. Math. Phys.* **342**, 47 (2016).
- [15] K. Sheshadri, H. R. Krishnamurthy, R. Pandit, and T. V. Ramakrishnan, Percolation-enhanced localization in the disordered Bosonic Hubbard model, *Phys. Rev. Lett.* **75**, 4075 (1995).
- [16] R. V. Pai, J. M. Kurdestany, K. Sheshadri, and R. Pandit, Bose-Hubbard models in confining potentials: Inhomogeneous mean-field theory, *Phys. Rev. B* **85**, 214524 (2012).
- [17] L. Lovász and B. Szegedy, Limits of dense graph sequences, *J. Comb. Theory, Ser. B* **96**, 933 (2006).
- [18] P. J. Wolfe and S. C. Olhede, Nonparametric graphon estimation, [arXiv:1309.5936](https://arxiv.org/abs/1309.5936).
- [19] A. Lipowski, D. Lipowska, and A. L. Ferreira, Phase transition and power-law coarsening in an Ising-doped voter model, *Phys. Rev. E* **96**, 032145 (2017).
- [20] D. Stauffer, Social applications of two-dimensional Ising models, *Am. J. Phys.* **76**, 470 (2008).
- [21] J. Majewski, H. Li, and J. Ott, The Ising model in physics and statistical genetics, *Am. J. Hum. Genet.* **69**, 853 (2001).
- [22] We point out that the Hamiltonian in Eq. (1) is invariant under $A_{G_L} \rightarrow A_{G_L} A$, $J^\alpha \rightarrow J^\alpha/c$. This degree of freedom on the graphon and $P_{n,v}$ is trivial because it does not affect its functional form, which is what governs the resulting equilibrium physics.
- [23] A. Bovier and V. Gayrard, The thermodynamics of the Curie-Weiss model with random couplings, *J. Stat. Phys.* **72**, 643 (1993).
- [24] J. I. Latorre, R. Orús, E. Rico, and J. Vidal, Entanglement entropy in the Lipkin-Meshkov-Glick model, *Phys. Rev. A* **71**, 064101 (2005).
- [25] K. Xu, Z.-H. Sun, W. Liu, Y.-R. Zhang, H. Li, H. Dong, W. Ren, P. Zhang, F. Nori, D. Zheng, H. Fan, and H. Wang, Probing dynamical phase transitions with a superconducting quantum simulator, *Sci. Adv.* **6**, eaba4935 (2020).
- [26] K. Binder and A. P. Young, Spin glasses: Experimental facts, theoretical concepts, and open questions, *Rev. Mod. Phys.* **58**, 801 (1986).
- [27] R. Harris *et al.*, Phase transitions in a programmable quantum spin glass simulator, *Science* **361**, 162 (2018).
- [28] J. Tindall, A. Searle, A. Alhajri, and D. Jaksch, Quantum physics in connected worlds, *Nat. Commun.* **13**, 7445 (2022).
- [29] M. Nazam and M. Arshad, On a fixed point theorem with application to integral equations, *Int. J. Analysis* **2016**, 9843207 (2016).
- [30] S. R. White, Density matrix formulation for quantum renormalization groups, *Phys. Rev. Lett.* **69**, 2863 (1992).
- [31] S. Chan and E. Airoldi, in *Proceedings of the 31st International Conference on Machine Learning*, edited by E. P. Xing and T. Jebara, Proceedings of Machine Learning Research Vol. 32 (PMLR, Beijing, China, 2014), pp. 208–216.
- [32] C. Borgs, J. Chayes, and A. Smith, in *Advances in Neural Information Processing Systems*, edited by C. Cortes, N. Lawrence, D. Lee, M. Sugiyama, and R. Garnett (Curran Associates, Montreal, Canada, 2015), Vol. 28.

- [33] J. Xu, in *Proceedings of the 35th International Conference on Machine Learning*, edited by J. Dy and A. Krause, Proceedings of Machine Learning Research Vol. 80 (PMLR, Stockholm Sweden, 2018), pp. 5433–5442.
- [34] M. Fishman, S. R. White, and E. M. Stoudenmire, The ITensor software library for tensor network calculations, *SciPost Phys. Codebases* **4** (2022).
- [35] E. Abbe, *J. Mach. Learn. Res.* **18**, 1 (2018), <http://jmlr.org/papers/v18/16-480.html>.
- [36] C. Borgs, J. Chayes, L. Lovász, V. Sós, and K. Vesztegombi, Limits of randomly grown graph sequences, *Eur. J. Combinat.* **32**, 985 (2011).
- [37] J. Hale and S. Lunel, *Introduction to Functional Differential Equations*, Applied Mathematical Sciences (Springer, New York, 2013).
- [38] L. Lovasz, *Large Networks and Graph Limits* (American Mathematical Society, Providence, RI, 2012).